

PointCaM: Cut-and-Mix for Open-Set Point Cloud Learning

Jie Hong^{a,b,1,2}, Shi Qiu^{a,b,1}, Weihao Li^a, Saeed Anwar^d, Mehrtash Harandi^c, Nick Barnes^a, Lars Petersson^b

^aAustralian National University, Canberra, Acton 2601, Australia

^bData61, CSIRO, Canberra, Acton 2601, Australia

^cMonash University, Wellington Rd, Clayton VIC 3800, Australia

^dInformation and Computer Science, King Fahd University of Petroleum&Minerals, Dhahran, 31261, Kingdom of Saudi Arabia

Abstract

Point cloud learning is receiving increasing attention, however, most existing point cloud models lack the practical ability to deal with the unavoidable presence of unknown objects. This paper mainly discusses point cloud learning under open-set settings, where we train the model without data from unknown classes and identify them in the inference stage. Basically, we propose to solve open-set point cloud learning using a novel Point Cut-and-Mix mechanism consisting of Unknown-Point Simulator and Unknown-Point Estimator modules. Specifically, we use the Unknown-Point Simulator to simulate out-of-distribution data in the training stage by manipulating the geometric context of partial known data. Based on this, the Unknown-Point Estimator module learns to exploit the point cloud's feature context for discriminating the known and unknown data. Extensive experiments show the plausibility of open-set point cloud learning and the effectiveness of our proposed solutions. Our code is available at <https://github.com/ShiQiu0419/pointcam>.

Keywords: 3D Point Clouds, Open-Set Recognition

Email addresses: jie.hong@anu.edu.au (Jie Hong), shi.qiu@anu.edu.au (Shi Qiu), weihao.lil@anu.edu.au (Weihao Li), saeed.anwar@kfupm.edu.sa (Saeed Anwar), mehrtash.harandi@monash.edu (Mehrtash Harandi), nick.barnes@anu.edu.au (Nick Barnes), lars.petersson@data61.csiro.au (Lars Petersson)

¹Equal contributions.

²Corresponding author.

1. Introduction

To better illustrate complicated scenes in the real-world, 3D data has been widely investigated in computer vision research. As a fundamental representation of 3D data, point clouds that can be collected from 3D scanners [1, 2] have shown great potential in AI-related applications, such as robotics [3, 4], remote sensing [5], and augmented/virtual reality [6].

Recent works [7, 8, 9, 10] leverage *data-driven* neural networks to analyze the context of 3D point clouds. Particularly, large-scale labeled point cloud data plays a crucial role in impacting the performance of deep networks. Despite the fast development in 3D sensing technology, point cloud data still requires expensive equipment for collection and huge human resources for annotation. The training datasets are assumed to contain all pre-defined object classes in the scenes; however, it is impractical to cover all possible classes in the real world. Thus, the richness and diversity of point cloud data are usually insufficient, especially for analyzing large-scale scenes [11, 12] and a wide variety of objects [13, 14]. Moreover, the effectiveness of point cloud data is also limited by its inherent sparsity and irregularity, which cause further challenges in common visual tasks such as point cloud classification [7, 15], segmentation [16, 17], and detection [18, 19].

The state-of-the-art point cloud learning models [7, 8, 17, 20, 21, 22] mainly focus on closed-set environments. These works often make a strong assumption that the object classes known during the deployment stage are only those provided during the training stage. However, this closed-set assumption is too restrictive, since in real-world environments the autonomous systems will unavoidably present unknown object classes that are not part of the training data. Currently, open-set recognition in the 2D image domain is active [23, 24, 25, 26], while the open-set learning of 3D point clouds is not commonly studied. In fact, this study has significant value in real-world applications. A possible outdoor scenario applies in self-driving, where an intelligent system may confront some objects that have not been seen before. By leveraging 3D open-set settings, the intelligent system can effectively identify such unknown objects, making drivers aware of the surroundings. Another potential use case for our 3D open-set settings is in XR (extended reality) systems. When a user is immersed in an XR gaming environment at home, the sudden appearance of a cat or a baby in the guarded area could pose a safety risk. However, traditional alerting mechanisms may not detect these unexpectedly moving creatures as their detection algorithms are trained

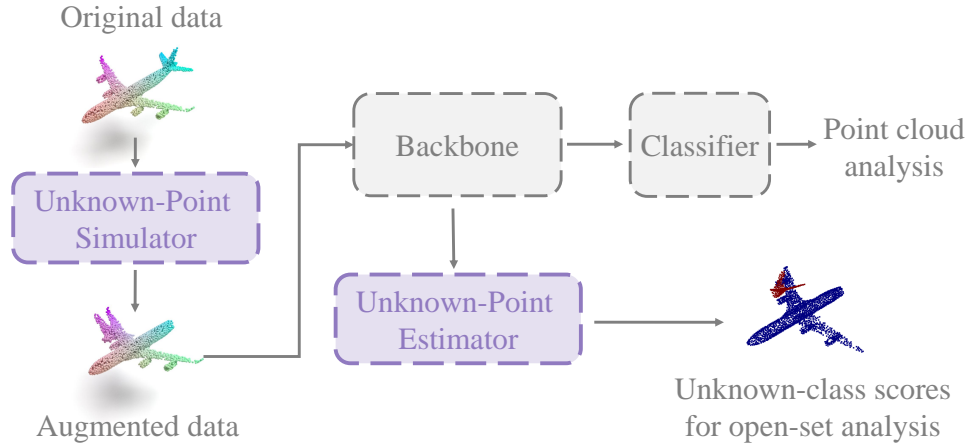


Figure 1: The PointCaM mechanism consists of two main modules: the Unknown-Point Simulator (UPS) simulates the out-of-distribution data during the training, and the Unknown-Point Estimator (UPE) is responsible for computing the unknown-class scores.

on regular indoor furniture and objects under closed-set settings. By incorporating our proposed settings and solutions, the XR system can easily recognize such “unknown” creatures, thereby increasing the robustness and effectiveness of the alerting mechanism. Given the promises in academic research and real-world applications, we explore open-set point cloud learning by enhancing the models’ abilities to deal with the inevitable unknown objects in 3D point cloud data.

Recently, a few studies investigate 3D data under open-set settings [27, 28]. For example, [29] addressed the few-shot 3D semantic segmentation task under an open-set setting, which presents an attention-aware multi-prototype transductive inference method. The target of [30] is unknown instance recognition under self-driving scenarios, where a feature predictor for anchors is designed to fit the characteristics of LiDAR data. Cen *et al.* [31] study *open-set LiDAR point cloud detection* through metric learning to overcome the problem of massive false positive detection samples. Moreover, [32] explores *open-world LiDAR segmentation*, where a redundancy classifier framework adapts the model to the open-set setting and incremental learning tasks. However, these works have some limitations that restrict general open-set 3D performance. First, methods [29, 30, 31, 33] lack simulated data about unknown classes, which impacts the model’s sensitivity to unknown objects. Second, [30, 31, 32, 33] only focus on the classifier’s features for recognizing unknown objects while neglecting information from the data and

learned feature maps.

To address the above limitations, in this work, we introduce a novel Point Cut-and-Mix (PointCaM) mechanism for open-set 3D point cloud learning. As illustrated in Fig. 1, PointCaM incorporates two main modules: Unknown-Point Simulator (UPS)³ and Unknown-Point Estimator (UPE)⁴. During the training process, we leverage the Unknown-Point Simulator to simulate out-of-distribution data by partially manipulating the geometric context of point clouds. To further discriminate the known and unknown objects provided by the UPS module, our UPE is designed to calculate an unknown-class score for each point. In particular, the UPE module estimates the unknown-class scores by adaptively fusing the multi-level feature context of point cloud data to learn the geometric dependencies and semantic correlations between known and unknown data.

The main contributions of this paper are summarized as follows: (1) We design a novel mechanism, PointCaM, for open-set point cloud learning. Two-component modules, the Unknown-Point Simulator (UPS) and the Unknown-Point Estimator (UPE) are proposed to simulate out-of-distribution data and estimate the unknown-class scores, respectively. (2) UPS helps to simulate out-of-distribution objects, where the selected point clouds are rotated and translated to exhibit highly distinct geometric distributions from known objects. (3) UPE adaptively fuses information from multiple feature encoding layers and computes the unknown scores. By utilizing information from both 3D coordinates and high-dimensional feature representations, UPE can leverage rich geometric and semantic contexts for differentiating between known and unknown objects.

2. Related Work

2.1. Open-Set Recognition

Although modern deep learning has demonstrated great success in closed-set visual recognition tasks, the challenge of open-set recognition has gained attention [34, 35, 36, 37]. In a closed-set image recognition scenario, the classifier aims to identify a set of image categories that remain consistent during both the training and testing phases. On the other hand, in an open-set image recognition scenario, the classifier must differentiate between the training categories and determine if an image belongs to an unknown class. In the case of object detection, open-set

³UPS for segmentation and Unknown-Sample Simulator (USS) for classification.

⁴UPE for segmentation and Unknown-Sample Estimator (USE) for classification. For simplicity, throughout the manuscript, we mainly use the terms: ‘unknown point’, ‘UPS’, and ‘UPE’.

detection [38, 39, 26] is designed to detect unknown objects from open-set data that includes both known and unknown objects. Similarly, in open-set semantic segmentation [40, 41], the goal is to segment an image containing known and unknown object classes. In addition to the task settings above, researchers have also been actively exploring the solutions in open-set learning, and recent studies have proposed methods like density estimation [23], uncertainty modeling [42], and input reconstruction [43] to identify open-set examples. For instance, [23] uses an encoder to encode the input data into a joint embedding space, a classifier to classify samples into known classes, and a flow-based density estimator to detect whether a sample belongs to the unknown class. [43] introduces a network architecture for open-set recognition that is based on learning reconstruction of input data and detects a given sample is an unknown by evaluating its inlier probability distribution. Nonetheless, all these studies still primarily concentrate on 2D recognition tasks and datasets, and open-set learning of 3D point clouds is rarely studied. In this work, we introduce a new 3D open-set setting for the point cloud domain.

According to different motivations, there are other problems, including out-of-distribution detection [42] and open-vocabulary recognition [44, 45], are closely related to open-set recognition. Out-of-distribution (OOD) detection focuses on detecting samples that are significantly different from the training data distribution [42, 46, 47]. For instance, [46] detects indoor objects (*i.e.*, OOD dataset) from outdoor 3D scenes. Open-vocabulary recognition classifies images by associating them with textual descriptions in a zero-shot manner using vision-language pretraining models, such as CLIP [44].

2.2. Point Cloud Learning

Following the success of Convolutional Neural Networks (CNNs) in image recognition, a number of papers [10] invent dedicated CNN-based models to analyze point cloud data. In general, point cloud learning relies highly on the learned point feature representations for accurate visual recognition. Recent networks can be categorized into two main streams: indirect and direct methods. Specifically, the indirect methods project original point clouds into certain intermediate representations, *e.g.*, multi-view images [48] or voxels [49], and apply regular 2D/3D CNNs to analyze the projected data. More recently, researchers tend to directly analyze given point cloud data using the tools of multi-layer perceptron MLP [7, 8], graph structure [50, 51], transformer [9, 52], *etc.* Compared to indirect methods, direct methods can save complicated data processing, avoid information loss, and benefit practical feasibility. In this work, we focus on direct open-set point cloud

learning, including the basic visual tasks of semantic segmentation and classification.

2.3. 3D Open-Set Settings

Recently, a few works addressed 3D data under open-set settings [27, 28]. The few-shot 3D semantic segmentation task under an open-set setting was first studied in [29], where an attention-aware multi-prototype transductive inference method is proposed. In [30], a feature predictor for anchors is specially designed to fit the characteristics of LiDAR data, targeting unknown instance recognition under self-driving scenarios. Cen *et al.* [31] study *open-set point cloud detection* via metric learning to overcome the problem of massive false positive detection samples in LiDAR-based data. Moreover, *open-world LiDAR segmentation* is explored in [32], where a redundancy classifier framework adapts the model to the open-set setting and incremental learning tasks. However, prior studies are subject to certain limitations: (1) methods in [29, 30, 31, 33] lack simulated data regarding unknown classes, which may impact the model’s sensitivity to unknown objects; and (2) [30, 31, 32, 33] only focus on the classifier’s features for recognizing unknown objects, while neglecting information from the data and learned feature maps. To address these limitations, our approach, PointCaM, utilizes parts of the point cloud to roughly approximate the unknown data. Specifically, we rotate and translate these point cloud sections to ensure sufficient geometric pattern differences from known objects. We then leverage the contextual information of the point cloud in both geometric and feature spaces to identify unknown data. Particularly, we adaptively fuse information from feature spaces with guidance from geometric space to compute the unknown score. The rich information concerning differences between known and unknown objects in such spaces enables the model to differentiate between the known and unknown categories more effectively.

Our work is done independently and concurrently with 3DOS [53] on a related benchmark. We summarize the main differences between the two works as follows: (1) Tasks. 3DOS only focuses on a specific open-set task, i.e. 3D object classification; in contrast, our benchmark covers a broad range of open-set 3D learning, including both 3D object classification and semantic segmentation. (2) Baselines. 3DOS only uses existing methods as the baselines in the benchmark. However, in our benchmark, we further propose a new open-set 3D learning method named PointCaM that outperforms these existing open-set methods. (3) Settings. Compared to the classification settings of 3DOS, to fit real-world scenarios, we divide the data into known and unknown classes where two split data include the classes of similar appearances.

2.4. *Cut-Mix Augmentation*

Cut-Mix and its related data augmentations present a simple way to improve visual recognition performance, including object detection [54], self-supervised representation learning [55], image classification [56], and anomaly detection [57]. For example, Cut-Paste-and-Learn [58] proposes to cut foreground object instances and paste them on diverse background images to synthesize object detection training images with bounding box labels. Copy-Paste [54] shows that applying random scale jittering on two random training images can significantly benefit training instance segmentation models. CutMix [56] cuts a rectangular image patch from an image and pastes it at a random location of another image. CutPaste [57] cuts an image patch and pastes it at a random location of the same image, producing spatial irregularities to estimate real defects. Inspired by the methods for image domain data augmentation, recent papers [59, 60, 61] have extended CutMix [56] to the point cloud domain for regular closed-set recognition tasks. In open-set recognition, data augmentations are used to generate samples that simulate the presence of out-of-distribution classes during training. This can help the model learn more robust features that are less specific to the known classes and more generalizable to new or unseen classes. For example, [62] introduces the counterfactual image generation augmentation which generates examples that are close to the training set examples yet do not belong to any training category using generative adversarial networks. Different from the existing works mentioned above, we present a Cut-and-Mix mechanism as a pioneering approach targeting open-set point cloud learning. Particularly, our proposed mechanism simulates the out-of-distribution data and enhances the models' capability of identifying the unknown data via a learnable module. Additionally, we propose learning an Unknown-Point Estimator module to exploit the point cloud's feature context for discriminating the known and unknown data.

3. **Problem Statement**

3.1. *Open-Set Point Cloud Learning*

Open-set point cloud learning includes two tasks: open-set point cloud segmentation and classification, where the objective is to assign an unknown score to each point (or sample). The deep model is trained solely on data from N_c known classes, but during evaluation, it must handle both N_c known and unknown classes. Assuming there is one unknown class, we calculate an unknown-class score, x (or x_{cls}), for each testing point (or sample) to estimate its probability of belonging to the unknown class. The overall performance of open-set point cloud

learning is measured based on the unknown-class scores of all testing points (or samples), denoted as $\{x_1, x_2, \dots, x_i, \dots\}$ (or $\{x_{cls,1}, x_{cls,2}, \dots, x_{cls,j}, \dots\}$). Ideally, if the i -th point (or j -th sample) belongs to the unknown class, we hope that x_i (or $x_{cls,j}$) approaches 1; while the point (or sample) belongs to the known classes, the corresponding score is expected to be 0. In summary, the goal of open-set point cloud learning is to train a network that can generate accurate unknown scores for each point (or sample).

3.2. Benchmarks

We adopt three widely used point cloud learning datasets, S3DIS [11], ModelNet40 [13], and ScanObjectNN [63] to conduct our experiments on the proposed 3D open-set tasks. Specifically, S3DIS [11] dataset contains 6 large-scale workspace point cloud scans, which can be further divided into 272 different rooms illustrating lobby, office, hallway, conference room, *etc.* In each room, about 0.5 to 2.5 million points are labeled into 13 classes for semantic segmentation. ModelNet40 [13] consists of 12,311 synthetic 3D object meshes in 40 different categories, where the corresponding point cloud data is sampled from the surface of each object mesh via uniform sampling. Following the common practice in the previous classification works [7, 8], about 9,843 point clouds are used for training, while the rest 2,468 samples are reserved for testing. As a real-world counterpart of ModelNet40, the ScanObjectNN [63] dataset incorporates a total of 14,298 manually collected point clouds in 15 object categories. Given the official data split in [63], the training set is composed of 11,416 samples, while the remaining 2,882 samples are utilized for testing purpose. To better evaluate our approaches, we conduct the open-set experiments under a more challenging case using the hardest perturbation variant of ScanObjectNN data [63].

In this open-set study, we customize each dataset by manually dividing the original data into known and unknown classes based on the given semantic labels. For open-set point cloud semantic segmentation, we borrow the idea of splitting classes in [64] where a few ‘thing’ classes are chosen as unknown classes. Practically, in the ‘Manual-10-3’ split of S3DIS, we choose three ‘thing’ classes of ‘table,’ ‘chair,’ and ‘sofa’ to form the unknown class, while in the ‘Manual-12-1’ split, only ‘sofa’ is selected as the unknown class. For open-set point cloud classification, we divide each original dataset (ModelNet40 [13] or ScanObjectNN [63]) into two splits, ModelNet40-*Split1* (or ScanObjectNN-*Split1*) and ModelNet40-*Split2* (or ScanObjectNN-*Split2*). In particular, we purposely separate classes with similar appearances in different splits to increase the task difficulty. Suppose the data chosen as the unknown class has similar attributes to the data pre-defined as

the known classes, then it is more challenging for the models to distinguish between the unknown and the known classes. More details of splits are provided in the supplementary material.

3.3. Evaluations

Both closed-set and open-set metrics are evaluated in our experiments. We choose mIoU and classification accuracy as the closed-set metrics. The standard open-set metrics for 2D tasks are included as open-set metrics: the false positive rate at 95% true positive rate (FPR at 95% TPR), the area under receiver operating characteristics (AUROC) [65, 66] and the area under the precision-recall (AUPR) [67, 68]. Such metrics assess the performance based on the overlap of unknown-class score distributions between the known and unknown classes. We hope to boost the models’ open-set performance while maintaining the closed-set classification accuracy. In other words, the model is expected to identify unknown objects and correctly classify known ones.

4. Methodology

4.1. Baseline Method

We adopt the training process of regular point cloud learning in the baseline models. Regarding the testing process, we borrow ideas from 2D tasks to compute the unknown-class scores. Specifically, we employ Maximum Softmax Probability (MSP) [69] or Maximum Unnormalized Logit (MaxLogit) [40] to calculate an unknown-class score x_i (or $x_{cls,j}$) for each point (or sample), based on its corresponding confidence or logit vector in the classifier.

4.2. PointCaM Mechanism

Given a point cloud containing N points, we describe the 3D coordinates $\mathcal{P} \in \mathbb{R}^{N \times 3}$ as the *geometric* context, which is explicitly collected by scanners indicating the geometric distribution of points in the original 3D space. In addition, the *feature* context $\mathcal{F} \in \mathbb{R}^{N \times C}$ of point cloud can be implicitly learned via CNN-based operations/modules from both local and global perspectives [70, 71], representing the latent semantic information in a C -dimensional feature space. In general, the geometric context \mathcal{P} and the feature context \mathcal{F} are considered as two main properties of point cloud data [17, 15], benefiting comprehensive point feature representations for accurate visual analysis. Based on these two properties, we propose a novel self-supervised approach, the PointCaM mechanism, to enhance open-set point cloud learning.

The PointCaM mechanism is illustrated in Fig. 1. Firstly, the Unknown-Point Simulator (UPS) or USS is applied to partially manipulate the geometric context, simulating unknown objects for training purposes. Secondly, a CNN-based Unknown-Point Estimator (UPE) or USE learns to discriminate between known and unknown objects by exploiting the feature context heavily. Compared to the baseline method mentioned above, our PointCaM not only additionally simulates out-of-distribution data for better training perception but also extracts more semantically meaningful feature information from the intermediate encoders rather than the output classifiers.

4.2.1. Unknown-Point Simulator

Our main concern lies in how to simulate out-of-distribution objects, while only known data are available during the training process. As mentioned above, the geometric context of point cloud data indicates the original distribution of known objects in 3D space; if we alter the geometric context to a certain extent, part of known data would become *unfamiliar* to a CNN’s perception since the distribution of points partially changes. Using this approach, we propose Alg. 1 to generate a *partial* geometric context.

Algorithm 1 Unknown-Point Simulator (UPS)

input: a point cloud $\mathcal{P} \in \mathbb{R}^{N \times 3}$
output: an augmented point cloud $\mathcal{Q} \in \mathbb{R}^{N \times 3}$
Randomly select a seed point s
1. $s = \mathbf{Rand}(\mathcal{P}) \in \mathbb{R}^3$
Find the k nearest neighbors of s
2. $\mathcal{C} = \mathbf{Knn}(s, \mathcal{P}) \in \mathbb{R}^{k \times 3}$
Augment \mathcal{C} by rotation and translation
3. $\mathcal{C}' = \mathbf{Aug}(\mathcal{C}) = T + R \cdot \mathcal{C} \in \mathbb{R}^{k \times 3}$
Cut \mathcal{C} from \mathcal{P} , and mix with \mathcal{C}'
4. $\mathcal{Q} = \mathbf{CutMix}(\mathcal{C}, \mathcal{P}, \mathcal{C}') \in \mathbb{R}^{N \times 3}$

At first, we randomly select (**‘Rand’**) a point $s \in \mathbb{R}^3$ from original point cloud $\mathcal{P} \in \mathbb{R}^{N \times 3}$ as a seed point. Then, we search for the neighbors of s as a subset of points $\mathcal{C} \in \mathbb{R}^{k \times 3}$ that we aim to augment. In practice, we apply the k -nearest-neighbors (**‘Knn’**) algorithm [50] to find a set of k neighbors based on the point-wise Euclidean-distances in 3D space. Particularly, the number of neighbors follows $k = \beta \cdot N$, where the selection ratio β is randomly drawn from

$[\beta_{min}, \beta_{max}]$ for a point cloud of N points. An ablation study about the maximum selection ratio $\beta_{max} \in (0, 1)$ is provided in Tab. 5. To augment (‘**Aug**’) \mathcal{C} as unknown points, we incorporate basic rotation and translation operations, considering two main benefits: (1) Compared to adding noise or scaling, it is a better way of simulating unknown objects as the natural local structures are preserved. This is evidenced by our experimental results presented in Tab. 4, where different regular transformations are performed to simulate unknown data points. Particularly, we observe that incorporating random rotation and translation can benefit the performance. The scaling operation shows a trivial effect while adding Gaussian noise causes inevitable damage to the local structures of an object and thus negatively impacts the performance. (2) Since only a subset of points ($k \ll N$) are modified with regular transformations while a majority of points remain unchanged, we ensure that for each point cloud sample, there is a proper proportion exists between known and unknown data points. This process is important to the 3D open-set settings: on the one hand, a small number of transformed points (*i.e.*, the ones simulated as “out-of-distribution data”) can help the model develop an additional capability of differentiating open-set data; on the other hand, a large number of unchanged points (*i.e.*, the ones used as “known data”) can help the model maintain its original capability of recognizing close-set data for regular 3D semantic segmentation and classification tasks. Specifically, $R \in \mathbb{R}^{3 \times 3}$ in Alg. 1 is a general rotation matrix representing three degree-of-freedom (3-DoF) random rotations, and $T \in \mathbb{R}^3$ is a 3-DoF random vector representing a further translation within the borders of \mathcal{P} . Finally, we drop the partial points \mathcal{C} in the original \mathcal{P} and keep the transformed \mathcal{C}' as the simulated out-of-distribution points, obtaining the partially altered geometric context $\mathcal{Q} \in \mathbb{R}^{N \times 3}$ that contains both known and unknown points (‘**CutMix**’).

Using the UPS module, the network is still trained with a standard segmentation or classification loss, *i.e.*, $\ell = \ell_{task}$. In open-set point cloud semantic segmentation, the selected points are assigned a label of $N_c + 1$, where N_c is the number of known classes. Similarly, in open-set point cloud classification, two samples of different known classes are partially cut, transformed, and mixed together to form a new sample labeled as $N_c + 1$, which introduces an additional class for unknown data in addition to the N_c known classes during training. The goal of UPS is to enrich the model’s knowledge of unknown objects, enhancing its sensitivity to such data. To achieve this, we generate unknown points in the data by manipulating parts of the original point cloud to ensure that the simulated out-of-distribution points have reasonable geometric features. Additionally, the rotation and translation of these points encourage an abnormal geometric distribution from

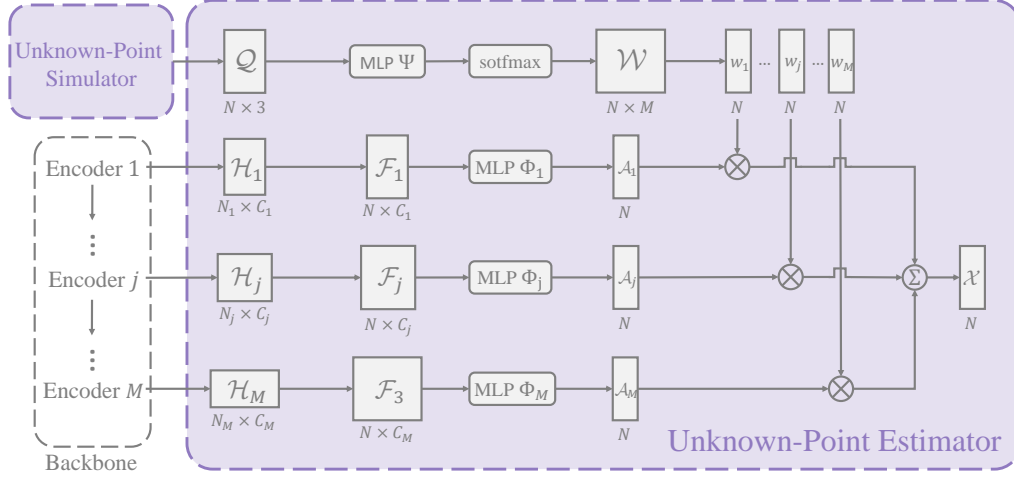


Figure 2: The detailed structure of the Unknown-Point Estimator (UPE). The figure illustrates the operations of the UPE module during the training process. For simplicity, we only demonstrate an example of fusing three intermediate feature maps. j is an arbitrary integer satisfying $1 \leq j \leq M$.

the known points.

Notably, since the UPS module simulates out-of-distribution data as a new class for training, one more dimension is added to the classifier’s output accordingly.

4.2.2. Unknown-Point Estimator

To discriminate the known and unknown points in \mathcal{Q} , a CNN-based Unknown-Point Estimator (UPE) module learns to compute accurate unknown-class scores by exploiting the feature context in the point cloud. As depicted in Fig. 2, given a baseline network, we denote the intermediate feature maps extracted from the baseline’s encoders as $\{\mathcal{H}_1, \dots, \mathcal{H}_j, \dots, \mathcal{H}_M\}$, where M is the number of intermediate feature maps and \mathcal{H}_j stands for an arbitrary one satisfying $1 \leq j \leq M$. Since a few point cloud networks [8, 16, 9] follow a U-Net [72] architecture to learn multi-level feature maps from lower point cloud resolutions (*i.e.*, $\mathcal{H}_j \in \mathbb{R}^{N_j \times C_j}$, where $N_j < N$), the extracted feature maps usually have different sizes. To restore the full feature context for all N points, we upsample $\{\mathcal{H}_1, \dots, \mathcal{H}_j, \dots, \mathcal{H}_M\}$ via the nearest neighbor interpolation method [17]. Then, the corresponding full-size feature context representations are obtained as $\{\mathcal{F}_1, \dots, \mathcal{F}_j, \dots, \mathcal{F}_M\}$, where $\forall \mathcal{F}_j \in \mathbb{R}^{N \times C_j}$.

Based on the feature context of $\{\mathcal{F}_1, \dots, \mathcal{F}_j, \dots, \mathcal{F}_M\}$, we intend to squeeze the

latent information and estimate a score x_i evaluating each point’s probability of whether it belongs to unknown data points. To achieve this, we apply a set of regular MLPs $\{\Phi_1, \dots, \Phi_j, \dots, \Phi_M\}$ to regress $\{\mathcal{F}_1, \dots, \mathcal{F}_j, \dots, \mathcal{F}_M\}$, respectively. For an arbitrary feature context \mathcal{F}_j , the estimated score vector is computed as $\mathcal{A}_j = \Phi_j(\mathcal{F}_j)$. Following similar computation, we acquire a set of score vectors $\{\mathcal{A}_1, \dots, \mathcal{A}_j, \dots, \mathcal{A}_M\}$, where $\forall \mathcal{A}_j \in \mathbb{R}^N$. Since the estimated score vectors are derived from different scales/levels of feature context representing a network’s hierarchical semantic information, it is necessary to synthesize them for a comprehensive prediction. Particularly, we leverage the altered geometric context \mathcal{Q} to guide an adaptive fusion of $\{\mathcal{A}_1, \dots, \mathcal{A}_j, \dots, \mathcal{A}_M\}$, because the simulated out-of-distribution data points are implied by their anomalous geometric distributions in 3D space compared to those given (known) points. To be concrete, we utilize another MLP Ψ followed by a channel-wise softmax function to learn the weight vectors:

$$\mathcal{W} = [w_1; \dots; w_j; \dots; w_M] = \text{softmax}(\Psi(\mathcal{Q})), \quad (1)$$

where $\mathcal{W} \in \mathbb{R}^{N \times M}$, and $\forall w_j \in \mathbb{R}^N$ represents a weight vector split from the columns of \mathcal{W} . Finally, we fuse the score vectors for all points as a weighted sum:

$$\mathcal{X} = \sum_{j=1}^M w_j \times \mathcal{A}_j, \quad \mathcal{X} \in \mathbb{R}^N. \quad (2)$$

The output vector \mathcal{X} ’s i -th scalar, x_i , corresponds to our computed unknown-class score on the i -th point q_i of \mathcal{Q} , indicating its possibility of being a simulated unknown data point. When training the UPE module, in addition to a typical task loss ℓ_{task} , the model is also subject to a mean squared error (MSE) loss ℓ_{upe} computed upon the UPE’s output score vector \mathcal{X} . The computation of ℓ_{upe} is formulated as:

$$\ell_{upe} = \frac{1}{N} \sum_{i=1}^N (x_i - \hat{x}_i)^2; \quad (3)$$

where the reference score $\hat{x}_i = 1$ if the point q_i is a simulated out-of-distribution data point; and $\hat{x}_i = 0$ if the point q_i belongs to one of the known classes. By minimizing the total loss $\ell = \ell_{task} + \alpha \cdot \ell_{upe}$ (α is an empirical parameter studied in Tab. 6) during the training stage, we enable the UPE module to differentiate between the unknown and known data points. In the testing stage, we directly calculate the unknown-class scores \mathcal{X} following Eq. 2, where the i -th scalar value x_i predicts the possibility of \mathcal{Q} ’s i -th point q_i belonging to the unknown class. For the semantic segmentation task, the unknown scores are calculated for all points

for prediction. The classification task further extracts an averaged unknown score over N points of the given sample for prediction.

UPE improves the open-set metric by investigating geometric dependencies and semantic connections between known and unknown points. To accomplish this, UPE employs an adaptive multi-level fusion module to distinguish between known and artificially generated unknown points. By examining point clouds and feature maps, UPE obtains more detailed information about the distinctions between known and unknown points. Compared to traditional multi-level prediction models [72, 73, 74] which only employ the feature maps, our UPE leverages the 3D geometric context of the point cloud for an adaptive multi-level fusion. This helps to adaptively and effectively integrate the multi-level semantic information in feature space, given the guidance of point cloud geometric structures in 3D space.

5. Experiments

Experiments have been carried out on two basic open-set point cloud learning tasks: point cloud semantic segmentation and classification. We test methods on the customized point cloud datasets: S3DIS-*Split* for open-set 3D semantic segmentation; ModelNet40-*Split* and ScanObjectNN-*Split* for open-set 3D classification. In general, we present rich experimental data to indicate the feasibility of our open-set settings for point cloud learning. Coupled with more ablation studies, our PointCaM mechanism is comprehensively verified using different benchmarks and backbone networks.

5.1. Implementations

In open-set 3D semantic segmentation experiments, k points are rotated and translated to mimic unknown points. Note $k = \beta \cdot N$ where $\beta \in [\beta_{min}, \beta_{max}]$ is the random selection ratio, and N is the number of total points of the point cloud. PointNet and PointNet++ are trained with 64 epochs using Adam optimizer [75]. The initial learning rate is set to 0.001. PointTransformer is trained with 100 epochs using SGD optimizer. The initial learning rate is 0.5. For open-set 3D classification, we first randomly choose samples to be augmented under an augmentation ratio of 0.1; then, for each chosen sample, we achieve the augmentation process by mixing it with k points that are randomly selected from another sample. Specifically, a total of k points can be selected from another sample of N points ($k = \beta \cdot N$). Then, we augment and mix these k neighbor points with the chosen sample points. A mixed sample will be used as a sample from the

unknown class. All classification models are trained with 300 epochs using an SGD optimizer. The number of total points, *i.e.* N , is set to 4096 and 1024 for open-set point cloud semantic segmentation and classification, respectively. We run all experiments using the GPU of NVIDIA GeForce RTX 3090.

In open-set point cloud semantic segmentation, we establish the selection ratio range $[\beta_{min}, \beta_{max}]$ of UPS at $[0.0, 0.6]$. Unlike classification on the sample level, we set β_{min} as 0.0 in semantic segmentation to facilitate the representation of unknown points at various sizes on the pixel level. The selection ratio range for open-set point cloud classification is set at $[0.4, 0.6]$. We set β_{min} and β_{max} values around 0.5 to ensure that the mixed unknown samples vary significantly from the original point cloud samples. The hyperparameter α , which determines the effect of the UPE module, is set to 5.0 and 1.0, for segmentation and classification tasks, respectively.

5.2. Open-Set 3D Semantic Segmentation

We first conduct open-set experiments on point cloud semantic segmentation, where the model intends to compute the unknown-class scores \mathcal{X} for all testing points. Here, we test our approaches using three popular backbones: the classical PointNet/PointNet++ [7, 8], and the advanced PointTransformer [9].

For most cases in Tab. 1, we observe that the UPS module clearly outperforms the MSP and MaxLogits baselines since the points simulated by the UPS contribute to modeling the unknown point sets during training. Furthermore, the designed UPE module also boosts the open-set metrics by a large margin. For instance, on the ‘Manual-10-3’ split with PointNet, UPS+MSP, and UPS+MaxLogits outperform basic MSP and MaxLogits by 3.6% and 7.0%, respectively; while a full PointCaM (UPS+UPE) mechanism achieves the best performance of 82.8%. When testing with PointTransformer, our PointCaM shows significant advantages over the basic MSP/MaxLogits and their incorporation with UPS. For example, on the ‘Manual-10-3’ of S3DIS-*Split*, we see PointCaM (UPS+UPE)’s $\sim 18\%$ and $\sim 12\%$ of AUROC improvements over MSP and UPS+MSP. Surprisingly, we notice that the network’s closed-set accuracies (mIoU) are simultaneously increased from 66.5/59.7% to 67.1%/61.6% with the help of the PointCaM. MLUC [31] outperforms MSP and MaxLogits with PointNet or PointNet++, but it achieves limited performance improvements using PointTransformer.

In addition to the quantitative results above, we have the following observations: (1) Though PointNet++ and PointTransformer show superior performance in closed-set metrics, they have inferior open-set ability. It indicates that, in 3D semantic segmentation, complicated neural networks make *overconfident* errors

and assign high-confidence predictions to unknown inputs. (2) For open-set problems, two key issues are about simulating the negative objects and exploring the spatial/semantic differences between positive and negative data. On the one hand, our UPS and UPE modules are designed to resolve each issue separately; on the other hand, since the UPE module relies on the UPS’s simulated objects to learn the discrepancies between unknown and known data, the proposed two modules also complement each other for accurate 3D open-set learning. (3) Tab. 1 shows that for PointNet on ‘Manual-12-1’, PointCaM does not outperform the baselines in AUPR. While this phenomenon is also observed in other works [40, 32], where a lower AUPR accompanies a higher AUROC, the underlying reason still requires further investigation. (4) Some visualization examples are compared and discussed in Figs. 3 and 4. The example in Fig. 4 showcases the density distributions of the scores for unknown-class samples. From the figure, it is evident that the separation between known and unknown points becomes more distinct when UPS is employed. That proves that UPS has the capability to simulate out-of-distribution points for the network, leading to an increased network sensitivity in identifying unknown points.

5.3. Open-Set 3D Classification

Moreover, we transfer our methods to open-set point cloud classification experiments. In addition to PointNet and PointNet++, we also utilize DGCNN [50] and AdaptConv [78] as testing backbones.

The quantitative results of open-set point cloud classification are reported in Tabs. 2 and 3, which show that the proposed methods consistently outperform the baseline method MSP in AUROC. For instance, compared to MSP and USS+MSP, the PointCaM (USS+USE) mechanism is marginally superior in AUROC on two datasets. It is worth noting that, in the ScanObjectNN-*Split* results of Tab. 3, the proposed USS+MSP and PointCaM (USS+USE) improve the open-set performance at a small cost to the closed-set accuracy. More experimental results and practical details are provided in the supplementary material.

5.4. Ablation Study

Unknown point generator. Here, we test multiple approaches to simulating unknown points: the single rotation within different angle ranges, the single translation within different ranges of the whole point cloud, the scaling, and the Gaussian noise. Simple rotation and translation can be considered special cases of our UPS when the translation vector is zero, or the rotation matrix is identity. Results in Tab. 4 show that UPS can effectively provide a valuable baseline for open-set point

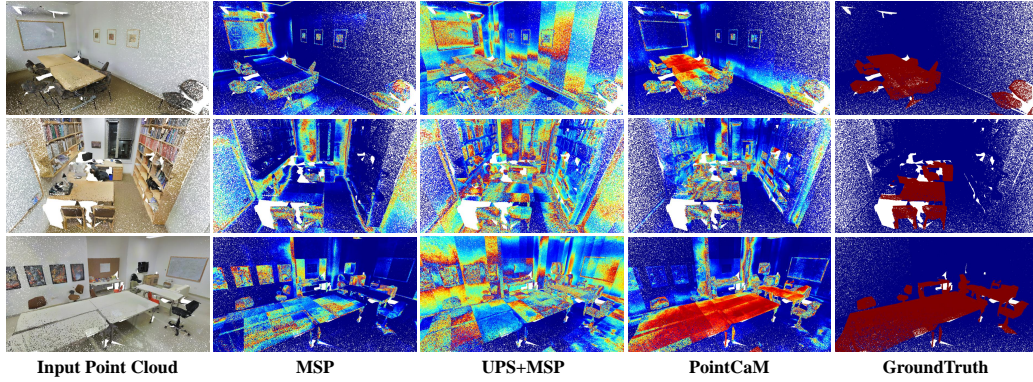


Figure 3: **The visualization examples: open-set point cloud semantic segmentation** of PointNet on S3DIS-*Split* with the ‘Manual-10-3’ split. Under the ‘Manual-10-3’ split, ‘table,’ ‘chair’ and ‘sofa’ are taken as unknown classes. We visualize heatmaps of estimated unknown-class scores using different open-set methods, *i.e.*, MSP [69], UPS+MSP, and our PointCaM (UPS+UPE). The ‘blue’ and ‘red’ points represent points from known and unknown classes. As we can observe in the second-column figures, the baseline MSP has the essential ability to recognize unknown objects. By using UPS, the model is endowed with superior perception ability for unknown points. For example, in the first-row figure, UPS+MSP identifies more parts of the ‘unknown table’ than MSP. However, the UPS module also causes a side effect on the models’ recognition confidence in known classes. To address this issue, the UPE module exploits the point cloud’s feature context by adaptively fusing the multi-scale feature maps. With the help of both the UPS and UPE modules, our proposed PointCaM mechanism well distinguishes the known and unknown points, as shown in the fourth-column figures.

cloud learning. Compared to other methods, UPS can generate unknown objects of natural and diverse appearances.

Sensitivity to parameters. There are two main hyper-parameters in the PointCaM mechanism: the maximum selection ratio β_{max} in the UPS module; and the coefficient of the MSE loss α in the UPE module. From Tabs. 5 and 6, models show sensitivity to these two parameters. The results in Tab. 5 show that with growing β_{max} , the open-set recognition ability of the model increases. Given the testing performances of α shown in Tab. 6, we empirically set the value $\alpha = 5.0$ for our experiments using the PointCaM mechanism. More ablations studies of experimental factors are presented in the supplementary material.

Fusion layers in UPE. In addition to UPS which simulates unknown points, we propose UPE to boost the open-set performance by exploiting the feature context in point clouds. In practice, UPE is designed to fuse the feature context from the encoders at different levels. We have an ablation study for UPE in Tab. 7, showing

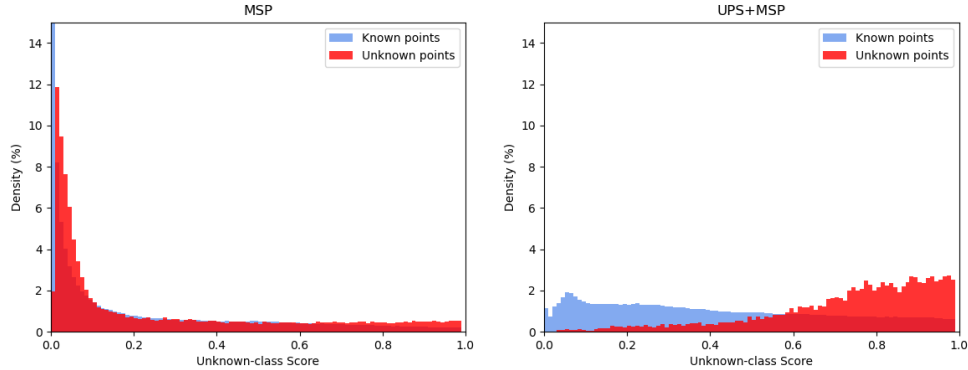


Figure 4: **The visualization examples: open-set point cloud semantic segmentation** of PointNet on S3DIS-*Split* with the ‘Manual-10-3’ split. We visualize the density distributions of the unknown-class score of MSP and UPS+MSP.

that its performance improves when difference levels of feature context are fused.

5.5. Discussion

Number of unknown classes. The results on S3DIS-*Split* (See Tab. 1) imply the negative impacts of unknown data on closed-set accuracy: increasing the number of unknown classes causes a worse closed-set accuracy. Thus, the mIoU values of the ‘Manual-10-3’ split are lower than that the ones reported in the ‘Manual-12-1’ split. This phenomenon is in line with the statements in [27, 24].

The 2D open-set methods. In Tab. 1, the incremental improvements produced by MSP [69] and MaxLogits [40] demonstrate that the 2D-driven methods also work for 3D point clouds. However, the performances in 2D and 3D cases are not consistent: *e.g.*, MaxLogits usually performs better than MSP in 2D tasks as [40] verifies; while in our 3D experiments, the performance of MaxLogits is worse than MSP (See Tab. 1). Similar observations showing possible incompatibility between 2D and 3D-driven open-set methods can be found in [32]. Directly adopting some 2D methods to 3D tasks might not be preferable due to point clouds’ unordered and unstructured characteristics. Thus, 3D-specific open-set methods such as our proposed PointCaM are worth further exploration.

Training time. In Tab. 8, we compare the training time and model size of various approaches with PointNet on ‘Manual-12-1’. The table shows that although there is a slight increase in model complexity, the substantial improvements in the open-set metric of our PointCaM model justify the extra complexity.

Other benchmarks. To showcase the practical effectiveness of PointCaM, we perform experiments on the SemanticKITTI autonomous driving dataset [79]. The results in Tab. 9 demonstrate that PointCaM achieves comparable performance in open-set metrics compared to other methods. We also evaluate our PointCaM on the 3DOS benchmark [53] for open-set point cloud classification. The results are presented in Tab. 10, where PointCaM delivers comparable performance to the best algorithms performed on the 3DOS benchmark.

Limitation. We identify the limitations of our work: (1) Although our empirical results demonstrate the superiority of our PointCaM model, the theoretical underpinnings of our findings require further development to better explain our observations. (2) In some instances, the close-set metrics are marginally inferior to those of the baseline. For example, as illustrated in Tab. 3, PointCaM with PointNet backbone attains an mIoU of 79.6% on ScanObjectNN-*Split2*, which is lower than 80.2% of MSP. Although this finding is consistent with some prior studies [81, 32], the reasons for this outcome require further investigation. (3) As observed in Tabs. 5 and 6, our proposed model appears to be somewhat sensitive to hyperparameters due to the inherent diversities of 3D point cloud data.

Performance drop. We conduct an experiment to investigate the cause of the performance drop, and the results are presented in Tab. 11. From the table, we observed that the open-set performance basically follows a similar trend to the closed-set performance. For instance, when AUROC drops significantly from 86.4% to 84.3%, the classification accuracy decreases by 0.5% from 97.7% to 97.2%. We also test more values of the augmentation ratio hyperparameter within a range of 0.01 to 0.2 and find that an increase in AUROC leads to slightly lower closed-set classification accuracy. Similar phenomena have been observed in prior studies [81, 32]. We hypothesize that as the model’s ability to distinguish unknown samples improves (indicated by an increase in AUROC), it becomes more cautious and makes more conservative decisions, *i.e.*, misclassifying some known samples as unknown ones. This hypothesis is further supported by the visualization in Fig 4, where a more distinct separation between known and unknown samples leads to lower confidence scores for the known samples. Additionally, in this case, the FPR (95% TPR) and Detection Error exhibit a similar trend to the classification accuracy.

6. Conclusion

This paper discusses point cloud learning under novel open-set settings. Two main point cloud visual analyzing tasks, semantic segmentation, and classifica-

tion, have been deeply investigated. To address the open-set point cloud problems, we propose a PointCaM mechanism to enhance a model’s capability of identifying unknown objects. Particularly, the UPS module helps to simulate the out-of-distribution data in the training stage, while the UPE module aims to exploit the fundamental context of point cloud data for accurate unknown-class score computation. By conducting extensive experiments and comprehensive ablation studies, we expect to inspire more future work on open-set point cloud problems.

References

- [1] F. Endres, J. Hess, J. Sturm, D. Cremers, W. Burgard, 3-d mapping with an rgb-d camera, *Transactions on Robotics* 30 (1) (2013) 177–187. [2](#)
- [2] M. Jaboyedoff, T. Oppikofer, A. Abellán, M.-H. Derron, A. Loye, R. Metzger, A. Pedrazzini, Use of lidar in landslide investigations: a review, *Natural hazards* 61 (1) (2012) 5–28. [2](#)
- [3] F. Pomerleau, F. Colas, R. Siegwart, et al., A review of point cloud registration algorithms for mobile robotics, *Foundations and Trends® in Robotics* 4 (1) (2015) 1–104. [2](#)
- [4] Y. Ze, N. Hansen, Y. Chen, M. Jain, X. Wang, Visual reinforcement learning with self-supervised 3d representations, *IEEE Robotics and Automation Letters* 8 (5) (2023) 2890–2897. [2](#)
- [5] W. Li, Q. Guo, M. K. Jakubowski, M. Kelly, A new method for segmenting individual trees from the lidar point cloud, *Photogrammetric Engineering & Remote Sensing* 78 (1) (2012) 75–84. [2](#)
- [6] Y. Chen, Q. Wang, H. Chen, X. Song, H. Tang, M. Tian, An overview of augmented reality technology, in: *Journal of Physics: Conference Series*, Vol. 1237, IOP Publishing, 2019, p. 022082. [2](#)
- [7] C. R. Qi, H. Su, K. Mo, L. J. Guibas, Pointnet: Deep learning on point sets for 3d classification and segmentation, in: *CVPR*, 2017, pp. 652–660. [2](#), [5](#), [8](#), [15](#), [29](#), [30](#), [32](#)
- [8] C. R. Qi, L. Yi, H. Su, L. J. Guibas, Pointnet++: Deep hierarchical feature learning on point sets in a metric space, in: *NIPS*, 2017, pp. 5099–5108. [2](#), [5](#), [8](#), [12](#), [15](#), [29](#), [30](#), [31](#), [33](#)

- [9] H. Zhao, L. Jiang, J. Jia, P. H. Torr, V. Koltun, Point transformer, in: Proceedings of the IEEE/CVF International Conference on Computer Vision, 2021, pp. 16259–16268. [2](#), [5](#), [12](#), [15](#), [29](#), [31](#)
- [10] Y. Guo, H. Wang, Q. Hu, H. Liu, L. Liu, M. Bennamoun, Deep learning for 3d point clouds: A survey, TPAMI (2020). [2](#), [5](#)
- [11] I. Armeni, S. Sax, A. R. Zamir, S. Savarese, Joint 2d-3d-semantic data for indoor scene understanding, arXiv:1702.01105 (2017). [2](#), [8](#)
- [12] J. Behley, M. Garbade, A. Milioto, J. Quenzel, S. Behnke, C. Stachniss, J. Gall, Semantickitti: A dataset for semantic scene understanding of lidar sequences, in: Proceedings of the IEEE/CVF International Conference on Computer Vision, 2019, pp. 9297–9307. [2](#)
- [13] Z. Wu, S. Song, A. Khosla, F. Yu, L. Zhang, X. Tang, J. Xiao, 3d shapenets: A deep representation for volumetric shapes, in: CVPR, 2015, pp. 1912–1920. [2](#), [8](#)
- [14] A. X. Chang, T. Funkhouser, L. Guibas, P. Hanrahan, Q. Huang, Z. Li, S. Savarese, M. Savva, S. Song, H. Su, et al., Shapenet: An information-rich 3d model repository, arXiv preprint arXiv:1512.03012 (2015). [2](#)
- [15] S. Qiu, S. Anwar, N. Barnes, Geometric back-projection network for point cloud classification, IEEE Transactions on Multimedia 24 (2021) 1943–1955. [2](#), [9](#)
- [16] C. Choy, J. Gwak, S. Savarese, 4d spatio-temporal convnets: Minkowski convolutional neural networks, in: CVPR, 2019. [2](#), [12](#)
- [17] Q. Hu, B. Yang, L. Xie, S. Rosa, Y. Guo, Z. Wang, N. Trigoni, A. Markham, Randla-net: Efficient semantic segmentation of large-scale point clouds, in: Proceedings of the IEEE/CVF Conference on Computer Vision and Pattern Recognition, 2020, pp. 11108–11117. [2](#), [9](#), [12](#)
- [18] S. Qiu, Y. Wu, S. Anwar, C. Li, Investigating attention mechanism in 3d point cloud object detection, in: 2021 International Conference on 3D Vision (3DV), IEEE, 2021, pp. 403–412. [2](#)
- [19] C. R. Qi, O. Litany, K. He, L. J. Guibas, Deep hough voting for 3d object detection in point clouds, in: proceedings of the IEEE/CVF International Conference on Computer Vision, 2019, pp. 9277–9286. [2](#)

- [20] W. Wang, R. Yu, Q. Huang, U. Neumann, Sgpn: Similarity group proposal network for 3d point cloud instance segmentation, in: Proceedings of the IEEE conference on computer vision and pattern recognition, 2018, pp. 2569–2578. [2](#)
- [21] S. Qiu, S. Anwar, N. Barnes, Semantic segmentation for real point cloud scenes via bilateral augmentation and adaptive fusion, in: Proceedings of the IEEE/CVF Conference on Computer Vision and Pattern Recognition, 2021, pp. 1757–1767. [2](#)
- [22] S. Qiu, S. Anwar, N. Barnes, Pu-transformer: Point cloud upsampling transformer, in: Proceedings of the Asian Conference on Computer Vision, 2022, pp. 2475–2493. [2](#)
- [23] H. Zhang, A. Li, J. Guo, Y. Guo, Hybrid models for open set recognition, in: European Conference on Computer Vision, Springer, 2020, pp. 102–117. [2](#), [5](#)
- [24] A. Dhamija, M. Gunther, J. Ventura, T. Boulton, The overlooked elephant of object detection: Open set, in: Proceedings of the IEEE/CVF Winter Conference on Applications of Computer Vision, 2020, pp. 1021–1030. [2](#), [18](#)
- [25] S. Kong, D. Ramanan, Opengan: Open-set recognition via open data generation, in: Proceedings of the IEEE/CVF International Conference on Computer Vision (ICCV), 2021, pp. 813–822. [2](#)
- [26] J. Zheng, W. Li, J. Hong, L. Petersson, N. Barnes, Towards open-set object detection and discovery, in: Proceedings of the IEEE/CVF Conference on Computer Vision and Pattern Recognition (CVPR) Workshops, 2022, pp. 3961–3970. [2](#), [5](#)
- [27] H. Ma, R. Xiong, Y. Wang, S. Kodagoda, L. Shi, Towards open-set semantic labeling in 3d point clouds: Analysis on the unknown class, *Neurocomputing* 275 (2018) 1282–1294. [3](#), [6](#), [18](#)
- [28] A. Bhardwaj, S. Pimpale, S. Kumar, B. Banerjee, Empowering knowledge distillation via open set recognition for robust 3d point cloud classification, *Pattern Recognition Letters* 151 (2021) 172–179. [3](#), [6](#)

- [29] N. Zhao, T.-S. Chua, G. H. Lee, Few-shot 3d point cloud semantic segmentation, in: Proceedings of the IEEE/CVF Conference on Computer Vision and Pattern Recognition, 2021, pp. 8873–8882. [3](#), [6](#)
- [30] K. Wong, S. Wang, M. Ren, M. Liang, R. Urtasun, Identifying unknown instances for autonomous driving, in: Conference on Robot Learning, PMLR, 2020, pp. 384–393. [3](#), [6](#)
- [31] J. Cen, P. Yun, J. Cai, M. Y. Wang, M. Liu, Open-set 3d object detection, in: 2021 International Conference on 3D Vision (3DV), IEEE, 2021, pp. 869–878. [3](#), [6](#), [15](#), [29](#)
- [32] J. Cen, P. Yun, S. Zhang, J. Cai, D. Luan, M. Y. Wang, M. Liu, M. Tang, Open-world semantic segmentation for lidar point clouds, arXiv preprint arXiv:2207.01452 (2022). [3](#), [6](#), [16](#), [18](#), [19](#), [29](#), [32](#)
- [33] H. Dong, Z. Chen, M. Yuan, Y. Xie, J. Zhao, F. Yu, B. Dong, L. Zhang, Region-aware metric learning for open world semantic segmentation via meta-channel aggregation, in: 31th International Joint Conference on Artificial Intelligence (IJCAI-22), 2022. [3](#), [6](#)
- [34] W. J. Scheirer, A. de Rezende Rocha, A. Sapkota, T. E. Boult, Toward open set recognition, IEEE transactions on pattern analysis and machine intelligence 35 (7) (2012) 1757–1772. [4](#)
- [35] A. Bendale, T. E. Boult, Towards open set deep networks, in: Proceedings of the IEEE Conference on Computer Vision and Pattern Recognition (CVPR), 2016. [4](#)
- [36] Y. Yang, C. Hou, Y. Lang, D. Guan, D. Huang, J. Xu, Open-set human activity recognition based on micro-doppler signatures, Pattern Recognition 85 (2019) 60–69. [4](#)
- [37] C. Geng, L. Tao, S. Chen, Guided cnn for generalized zero-shot and open-set recognition using visual and semantic prototypes, Pattern Recognition 102 (2020) 107263. [4](#)
- [38] A. Dhamija, M. Gunther, J. Ventura, T. Boult, The overlooked elephant of object detection: Open set, in: Proceedings of the IEEE/CVF Winter Conference on Applications of Computer Vision (WACV), 2020. [5](#)

- [39] K. Joseph, S. Khan, F. S. Khan, V. N. Balasubramanian, Towards open world object detection, in: Proceedings of the IEEE/CVF Conference on Computer Vision and Pattern Recognition, 2021, pp. 5830–5840. [5](#)
- [40] D. Hendrycks, S. Basart, M. Mazeika, A. Zou, J. Kwon, M. Mostajabi, J. Steinhardt, D. Song, Scaling out-of-distribution detection for real-world settings, in: Proceedings of the 39th International Conference on Machine Learning (ICML), PMLR, 2022, pp. 8759–8773. [5](#), [9](#), [16](#), [18](#), [29](#), [32](#)
- [41] J. Hong, W. Li, J. Han, J. Zheng, P. Fang, M. Harandi, L. Petersson, Goss: Towards generalized open-set semantic segmentation, arXiv preprint arXiv:2203.12116 (2022). [5](#)
- [42] S. Liang, Y. Li, R. Srikant, Enhancing the reliability of out-of-distribution image detection in neural networks, arXiv preprint arXiv:1706.02690 (2017). [5](#)
- [43] S. Pidhorskyi, R. Almhosen, G. Doretto, Generative probabilistic novelty detection with adversarial autoencoders, Advances in neural information processing systems 31 (2018). [5](#)
- [44] A. Radford, J. W. Kim, C. Hallacy, A. Ramesh, G. Goh, S. Agarwal, G. Sastry, A. Askell, P. Mishkin, J. Clark, et al., Learning transferable visual models from natural language supervision, in: International conference on machine learning, PMLR, 2021, pp. 8748–8763. [5](#)
- [45] H. Pham, Z. Dai, G. Ghiasi, K. Kawaguchi, H. Liu, A. W. Yu, J. Yu, Y.-T. Chen, M.-T. Luong, Y. Wu, et al., Combined scaling for open-vocabulary image classification, arXiv e-prints (2021) arXiv:2111. [5](#)
- [46] L. Veeramacheni, M. Valdenegro-Toro, A benchmark for out of distribution detection in point cloud 3d semantic segmentation, in: NeurIPS 2022 Workshop on Robot Learning: Trustworthy Robotics, 2022. [5](#)
- [47] M. Salehi, H. Mirzaei, D. Hendrycks, Y. Li, M. H. Rohban, M. Sabokrou, A unified survey on anomaly, novelty, open-set, and out of-distribution detection: Solutions and future challenges, Transactions of Machine Learning Research (2022). [5](#)

- [48] H. Su, S. Maji, E. Kalogerakis, E. Learned-Miller, Multi-view convolutional neural networks for 3d shape recognition, in: Proceedings of the IEEE international conference on computer vision, 2015, pp. 945–953. [5](#)
- [49] D. Maturana, S. Scherer, Voxnet: A 3d convolutional neural network for real-time object recognition, in: 2015 IEEE/RSJ international conference on intelligent robots and systems (IROS), IEEE, 2015, pp. 922–928. [5](#)
- [50] Y. Wang, Y. Sun, Z. Liu, S. E. Sarma, M. M. Bronstein, J. M. Solomon, Dynamic graph cnn for learning on point clouds, *Acm Transactions On Graphics (tog)* 38 (5) (2019) 1–12. [5](#), [10](#), [16](#), [30](#)
- [51] Y. Liu, B. Fan, S. Xiang, C. Pan, Relation-shape convolutional neural network for point cloud analysis, in: Proceedings of the IEEE/CVF Conference on Computer Vision and Pattern Recognition, 2019, pp. 8895–8904. [5](#)
- [52] M.-H. Guo, J.-X. Cai, Z.-N. Liu, T.-J. Mu, R. R. Martin, S.-M. Hu, Pct: Point cloud transformer, *Computational Visual Media* 7 (2) (2021) 187–199. [5](#)
- [53] A. Alliegro, F. Cappio Borlino, T. Tommasi, 3dos: Towards 3d open set learning-benchmarking and understanding semantic novelty detection on point clouds, *Advances in Neural Information Processing Systems* 35 (2022) 21228–21240. [6](#), [19](#), [33](#)
- [54] G. Ghiasi, Y. Cui, A. Srinivas, R. Qian, T.-Y. Lin, E. D. Cubuk, Q. V. Le, B. Zoph, Simple copy-paste is a strong data augmentation method for instance segmentation, in: Proceedings of the IEEE/CVF Conference on Computer Vision and Pattern Recognition (CVPR), 2021, pp. 2918–2928. [7](#)
- [55] J. Han, L. Petersson, H. Li, I. Reid, Cropmix: Sampling a rich input distribution via multi-scale cropping, *arXiv preprint arXiv:2205.15955* (2022). [7](#)
- [56] S. Yun, D. Han, S. J. Oh, S. Chun, J. Choe, Y. Yoo, Cutmix: Regularization strategy to train strong classifiers with localizable features, in: Proceedings of the IEEE/CVF International Conference on Computer Vision (ICCV), 2019. [7](#)
- [57] C.-L. Li, K. Sohn, J. Yoon, T. Pfister, Cutpaste: Self-supervised learning for anomaly detection and localization, in: Proceedings of the IEEE/CVF

- Conference on Computer Vision and Pattern Recognition (CVPR), 2021, pp. 9664–9674. [7](#)
- [58] D. Dwibedi, I. Misra, M. Hebert, Cut, paste and learn: Surprisingly easy synthesis for instance detection, in: Proceedings of the IEEE International Conference on Computer Vision (ICCV), 2017. [7](#)
- [59] E. Harris, A. Marcu, M. Painter, M. Niranjana, A. Prügel-Bennett, J. Hare, Fmix: Enhancing mixed sample data augmentation, arXiv preprint arXiv:2002.12047 (2020). [7](#)
- [60] D. Lee, J. Lee, J. Lee, H. Lee, M. Lee, S. Woo, S. Lee, Regularization strategy for point cloud via rigidly mixed sample, in: Proceedings of the IEEE/CVF Conference on Computer Vision and Pattern Recognition, 2021, pp. 15900–15909. [7](#)
- [61] J. Zhang, L. Chen, B. Ouyang, B. Liu, J. Zhu, Y. Chen, Y. Meng, D. Wu, Pointcutmix: Regularization strategy for point cloud classification, Neurocomputing (2022). [7](#)
- [62] L. Neal, M. Olson, X. Fern, W.-K. Wong, F. Li, Open set learning with counterfactual images, in: Proceedings of the European Conference on Computer Vision (ECCV), 2018, pp. 613–628. [7](#)
- [63] M. A. Uy, Q.-H. Pham, B.-S. Hua, T. Nguyen, S.-K. Yeung, Revisiting point cloud classification: A new benchmark dataset and classification model on real-world data, in: Proceedings of the IEEE/CVF international conference on computer vision, 2019, pp. 1588–1597. [8](#)
- [64] J. Cen, P. Yun, J. Cai, M. Y. Wang, M. Liu, Deep metric learning for open world semantic segmentation, in: Proceedings of the IEEE/CVF International Conference on Computer Vision, 2021, pp. 15333–15342. [8](#)
- [65] J. Davis, M. Goadrich, The relationship between precision-recall and roc curves, in: Proceedings of the 23rd international conference on Machine learning, 2006, pp. 233–240. [9](#)
- [66] T. Fawcett, An introduction to roc analysis, Pattern recognition letters 27 (8) (2006) 861–874. [9](#)

- [67] C. Manning, H. Schütze, Foundations of statistical natural language processing, MIT press, 1999. [9](#)
- [68] T. Saito, M. Rehmsmeier, The precision-recall plot is more informative than the roc plot when evaluating binary classifiers on imbalanced datasets, PloS one 10 (3) (2015) e0118432. [9](#)
- [69] D. Hendrycks, K. Gimpel, A baseline for detecting misclassified and out-of-distribution examples in neural networks, in: ICLR, 2017. [9](#), [17](#), [18](#), [29](#), [30](#), [32](#)
- [70] X. Yan, C. Zheng, Z. Li, S. Wang, S. Cui, Pointasnl: Robust point clouds processing using nonlocal neural networks with adaptive sampling, in: Proceedings of the IEEE/CVF Conference on Computer Vision and Pattern Recognition, 2020, pp. 5589–5598. [9](#)
- [71] S. Qiu, S. Anwar, N. Barnes, Pnp-3d: A plug-and-play for 3d point clouds, IEEE Transactions on Pattern Analysis and Machine Intelligence (2021). [9](#)
- [72] O. Ronneberger, P. Fischer, T. Brox, U-net: Convolutional networks for biomedical image segmentation, in: International Conference on Medical image computing and computer-assisted intervention, Springer, 2015, pp. 234–241. [12](#), [14](#)
- [73] J. Long, E. Shelhamer, T. Darrell, Fully convolutional networks for semantic segmentation, in: Proceedings of the IEEE conference on computer vision and pattern recognition, 2015, pp. 3431–3440. [14](#)
- [74] C.-Y. Lee, S. Xie, P. Gallagher, Z. Zhang, Z. Tu, Deeply-supervised nets, in: Artificial intelligence and statistics, PMLR, 2015, pp. 562–570. [14](#)
- [75] D. P. Kingma, J. Ba, Adam: A method for stochastic optimization, arXiv preprint arXiv:1412.6980 (2014). [14](#)
- [76] S. Vaze, K. Han, A. Vedaldi, A. Zisserman, Open-set recognition: A good closed-set classifier is all you need, in: International Conference on Learning Representations, 2021. [30](#)
- [77] R. Huang, A. Geng, Y. Li, On the importance of gradients for detecting distributional shifts in the wild, Advances in Neural Information Processing Systems 34 (2021) 677–689. [30](#)

- [78] H. Zhou, Y. Feng, M. Fang, M. Wei, J. Qin, T. Lu, Adaptive graph convolution for point cloud analysis, in: Proceedings of the IEEE/CVF International Conference on Computer Vision, 2021, pp. 4965–4974. [16](#), [30](#)
- [79] J. Behley, M. Garbade, A. Milioto, J. Quenzel, S. Behnke, C. Stachniss, J. Gall, SemanticKITTI: A Dataset for Semantic Scene Understanding of LiDAR Sequences, in: Proc. of the IEEE/CVF International Conf. on Computer Vision (ICCV), 2019. [19](#), [32](#)
- [80] Y. Gal, Z. Ghahramani, Dropout as a bayesian approximation: Representing model uncertainty in deep learning, in: international conference on machine learning, PMLR, 2016, pp. 1050–1059. [32](#)
- [81] G. Chen, P. Peng, X. Wang, Y. Tian, Adversarial reciprocal points learning for open set recognition, IEEE Transactions on Pattern Analysis and Machine Intelligence 44 (11) (2021) 8065–8081. [19](#)

Data Split	Backbone	Open-Set Method	Closed-Set Metric	Open-Set Metric			
			mIoU	FPR (95% TPR) ↓	AUPR ↑	AUROC ↑	
Manual-12-1	PointNet [7]	MSP [69]	48.8	47.1	0.9	81.3	
		MaxLogits [40]	48.8	45.5	1.3	82.3	
		MLUC [31]	46.2	42.4	1.2	82.9	
		REAL [32]	46.5	44.7	0.9	81.8	
		UPS+MSP	47.1	47.4	1.1	80.5	
		UPS+MaxLogits	47.1	45.3	1.0	81.4	
		PointCaM (Ours)	46.5	40.9	0.9	83.1	
	PointNet++ [8]	MSP [69]	52.8	93.4	0.3	51.3	
		MaxLogits [40]	52.8	92.7	0.3	48.8	
		MLUC [31]	52.5	93.1	0.4	53.9	
		REAL [32]	53.7	93.1	0.3	51.9	
		UPS+MSP	53.7	93.1	0.3	52.4	
		UPS+MaxLogits	53.7	93.4	0.3	50.8	
		PointCaM (Ours)	54.8	87.4	0.4	55.6	
	PointTransformer [9]	MSP [69]	66.5	100.0	13.3	59.0	
		MaxLogits [40]	66.5	99.8	13.4	59.3	
		MLUC [31]	65.5	99.9	13.8	59.2	
		REAL [32]	67.5	99.8	14.4	62.0	
		UPS+MSP	67.1	99.7	17.0	66.0	
		UPS+MaxLogits	67.1	90.1	18.2	65.4	
		PointCaM (Ours)	67.1	73.9	18.7	72.0	
	Manual-10-3	PointNet [7]	MSP [69]	45.4	63.0	9.1	68.1
			MaxLogits [40]	45.4	63.0	8.5	65.7
			MLUC [31]	44.4	46.4	15.8	74.3
REAL [32]			43.2	57.9	9.9	71.6	
UPS+MSP			44.1	58.5	10.0	71.7	
UPS+MaxLogits			44.1	56.2	10.4	72.7	
PointCaM (Ours)			43.8	42.0	19.8	82.8	
PointNet++ [8]		MSP [69]	48.7	93.4	6.5	52.6	
		MaxLogits [40]	48.7	94.9	6.4	51.3	
		MLUC [31]	47.4	93.4	7.7	57.2	
		REAL [32]	49.6	93.4	6.7	53.4	
		UPS+MSP	49.3	93.4	6.6	53.3	
		UPS+MaxLogits	49.3	93.4	6.9	54.1	
		PointCaM (Ours)	49.5	84.7	7.8	60.6	
PointTransformer [9]		MSP [69]	59.7	100.0	17.0	52.8	
		MaxLogits [40]	59.7	99.5	17.3	53.0	
		MLUC [31]	59.2	99.9	17.6	54.5	
		REAL [32]	61.3	99.9	19.5	58.9	
		UPS+MSP	60.0	99.8	19.5	59.0	
		UPS+MaxLogits	60.0	93.9	23.4	59.8	
		PointCaM (Ours)	61.6	74.1	26.5	70.7	

Table 1: **Open-Set Point Cloud Semantic Segmentation** on S3DIS-*Split* with PointNet, PointNet++ and PointTransformer. FPR (95% TPR), pixel-level AUPR, and AUROC in % are given. ‘PointCaM’ is equal to ‘UPS+UPE’. β_{max} and α are set to 0.6 and 5.0, respectively.

Backbone	Open-Set Method	Closed-Set Metric		Open-Set Metric		
		Accuracy (sample)	Accuracy (class)	FPR (95% TPR) ↓	Detection Error ↓	AUROC ↑
PointNet [7]	MSP [69]	96.1	94.3	49.9	17.6	89.0
	MLS [76]	96.1	94.3	50.7	16.9	88.8
	GradNorm [77]	96.1	94.3	48.0	17.7	88.0
	USS+MSP	96.1	93.8	47.4	17.1	90.2
	PointCaM (Ours)	96.0	94.1	43.7	17.1	90.2
PointNet++ [8]	MSP [69]	97.8	96.3	33.5	14.8	85.9
	MLS [76]	97.8	96.3	35.4	14.5	86.2
	GradNorm [77]	97.8	96.3	34.3	17.2	82.0
	USS+MSP	97.7	96.2	36.4	15.2	85.9
	PointCaM (Ours)	97.7	96.3	35.4	15.6	86.4
DGCNN [50]	MSP [69]	97.5	95.9	35.9	13.9	91.7
	MLS [76]	97.5	95.9	34.6	13.0	91.7
	GradNorm [77]	97.5	95.9	35.8	13.7	90.9
	USS+MSP	97.4	96.0	35.1	13.6	91.9
	PointCaM (Ours)	97.7	96.3	35.1	13.7	92.5
AdaptConv [78]	MSP [69]	97.8	96.3	33.0	14.6	90.6
	MLS [76]	97.8	96.3	34.7	13.5	89.6
	GradNorm [77]	97.8	96.3	34.9	14.8	90.6
	USS+MSP	97.9	96.4	33.1	14.4	91.8
	PointCaM (Ours)	97.9	96.6	33.6	14.2	91.9

Table 2: **Open-Set Point Cloud Classification** on ModelNet40-*Split*. The closed-set metrics, including classification accuracies over sample/class, and open-set metrics, including FPR (95% TPR), detection error, and image-level AUROC in %, are given. ‘PointCaM’ is equal to ‘USS+USE’. ModelNet40-*Split2* is taken as the training dataset, while ModelNet40-*Split2* plus -*Split1* is the evaluation dataset.

Backbone	Open-Set Method	Closed-Set Metric		Open-Set Metric		
		Accuracy (sample)	Accuracy (class)	FPR (95% TPR) ↓	Detection Error ↓	AUROC ↑
PointNet [7]	MSP [69]	80.2	75.7	86.8	39.7	63.6
	MLS [76]	80.2	75.7	89.9	42.2	60.4
	GradNorm [77]	80.2	75.7	87.6	39.4	64.0
	USS+MSP	79.3	75.5	90.5	40.5	63.3
	PointCaM (Ours)	79.6	75.6	86.0	38.6	65.5
PointNet++ [8]	MSP [69]	88.2	87.1	80.6	30.6	72.2
	MLS [76]	88.2	87.1	80.2	32.3	71.4
	GradNorm [77]	88.2	87.1	81.8	35.5	65.1
	USS+MSP	88.8	87.8	81.3	30.9	72.2
	PointCaM (Ours)	88.1	86.8	79.6	30.2	73.1
DGCNN [50]	MSP [69]	88.0	86.2	84.3	29.9	75.3
	MLS [76]	88.0	86.2	79.3	30.3	75.5
	GradNorm [77]	88.0	86.2	82.1	30.2	75.0
	USS+MSP	88.2	86.2	83.7	29.4	75.5
	PointCaM (Ours)	87.6	85.9	82.9	29.7	76.0
AdaptConv [78]	MSP [69]	87.5	85.5	86.7	31.1	73.4
	MLS [76]	87.5	85.5	85.0	30.5	74.4
	GradNorm [77]	87.5	85.5	85.2	30.4	74.2
	USS+MSP	86.8	84.6	84.6	30.4	74.1
	PointCaM (Ours)	87.1	85.5	84.1	30.1	74.4

Table 3: **Open-Set Point Cloud Classification** on ScanObjectNN-*Split*. The closed-set metrics, including classification accuracies over sample/class, and open-set metrics, including FPR (95% TPR), detection error, and image-level AUROC in %, are given. ‘PointCaM’ is equal to ‘USS+USE’. ScanObjectNN-*Split2* is taken as the training dataset, while ScanObjectNN-*Split2* plus -*Split1* is the evaluation dataset.

Data Split	Backbone	Open-Set Method	AUROC \uparrow
Manual-10-3	PointNet [7]	MSP	68.1
		MSP+single rotation (0.5π)	69.9
		MSP+single rotation (π)	70.4
		MSP+single rotation (2π)	70.9
		MSP+single translation (0.25 range)	63.9
		MSP+single translation (0.5 range)	69.5
		MSP+single translation (whole range)	70.8
		MSP+scaling	67.3
		MSP+Gaussian noise	58.1
		MSP+UPS	71.7

Table 4: **The ablation study:** Unknown point generator. PointNet is performed in Open-Set Point Cloud Semantic Segmentation on S3DIS-*Split*. The metric AUROC in % is given.

Data Split	Backbone	Open-Set Method	β_{max}	AUROC \uparrow
Manual-12-1	PointTransformer [9]	UPS+MSP	0.2	59.4
		UPS+MaxLogits		62.3
		UPS+MSP	0.3	62.8
		UPS+MaxLogits		64.7
		UPS+MSP	0.4	61.6
		UPS+MaxLogits		64.6
		UPS+MSP	0.5	63.5
		UPS+MaxLogits		65.1
		UPS+MSP	0.6	66.0
		UPS+MaxLogits		65.4
		UPS+MSP	0.7	65.5
		UPS+MaxLogits		65.0

Table 5: **The ablation study:** β_{max} . PointTransformer is performed in Open-Set Point Cloud Semantic Segmentation on S3DIS-*Split*. The metric AUROC in % is given.

Data Split	Backbone	Open-Set Method	α	AUROC \uparrow
Manual-10-3	PointNet++ [8]	PointCaM	0.2	56.8
			1.0	59.5
			2.5	58.6
			5.0	60.6
			7.5	57.0
			10.0	58.3
			12.5	56.6
			15.0	55.5

Table 6: **The ablation study:** α . PointNet++ is performed in Open-Set Point Cloud Semantic Segmentation on S3DIS-*Split*. The metric AUROC in % is given.

Data Split	Backbone	Open-Set Method	Fusion Layer	AUROC \uparrow
Manual-10-3	PointNet [7]	PointCaM	-	68.1
			1st layer	78.8
			1st+2nd layers	81.2
			1st+2nd+3rd layers (w/o point-guided fusion)	79.9
			1st+2nd+3rd layers (with point-guided fusion)	82.8

Table 7: **The ablation study:** Fusion layers in UPE. PointNet++ is performed in Open-Set Point Cloud Semantic Segmentation on S3DIS-*Split*. The metric AUROC in % is given.

Data Split	Backbone	Open-Set Method	Model Complexity		Open-Set Metric
			Training Time	Params	AUROC \uparrow
Manual-10-3	PointNet [7]	MSP [69]	0.23s	41481K	68.1
		MaxLogits [40]	0.23s	41481K	65.7
		UPS+MSP	0.19s	41482K	71.7
		UPS+MaxLogits	0.19s	41482K	72.7
		PointCaM (Ours)	0.24s	41501K	82.8

Table 8: **Training time:** PointNet is performed in Open-Set Point Cloud Semantic Segmentation on S3DIS-*Split*. The training time for each iteration and model size are provided.

Dataset	SemanticKITTI			nuScenes		
	AUPR \uparrow	AUROC \uparrow	mIoU \uparrow	AUPR \uparrow	AUROC \uparrow	mIoU \uparrow
MSP [69]	6.7	74.0	58.0	4.3	76.7	58.7
MaxLogits [40]	7.6	70.5	58.0	8.3	79.4	58.7
MC-Dropout [80]	7.4	74.7	58.0	14.9	82.6	58.7
REAL [32]	20.8	84.9	57.8	21.2	84.5	56.8
PointCaM (Ours)	20.7	86.2	57.8	20.1	85.3	56.8

Table 9: **Ohter benchmarks:** Open-set point cloud semantic segmentation on SemanticKITTI [79]. AUPR, AUROC and mIoU in % are given. The hyperparameters β and α are set to 0.6 and 15.0.

Synth to Real Benchmark - DGCNN						
Method	SR 1 (easy)		SR 2 (hard)		Avg	
	AUROC \uparrow	FPR95 \downarrow	AUROC \uparrow	FPR95 \downarrow	AUROC \uparrow	FPR95 \downarrow
MSP	72.2	91.0	61.2	90.3	66.7	90.6
MLS	69.0	92.2	62.4	88.9	65.7	90.5
ODIN	69.0	92.2	62.4	89.0	65.7	90.6
Energy	68.8	92.7	62.4	88.9	65.6	90.8
GradNorm	67.0	93.5	59.8	89.4	63.4	91.5
ReAct	68.4	92.1	62.8	88.8	65.6	90.5
VAE	68.6	77.0	57.9	92.3	63.3	84.6
NF	72.5	81.6	70.2	83.0	71.3	82.3
OE+mixup	71.1	89.6	59.5	92.0	65.3	90.8
ARPL+CS	71.5	90.2	62.8	89.5	67.1	89.8
Cosine proto	58.6	90.6	57.3	91.3	57.9	91.0
CE	67.5	87.4	64.6	91.0	66.1	89.2
SubArcFace	74.5	86.7	68.7	86.6	71.6	86.7
PointCaM (Ours)	77.04	87.52	65.23	85.59	71.1	86.6

Table 10: **Ohter benchmarks:** Open-set point cloud classification on 3DOS (Synthetic to Real Benchmark track) [53]. The metrics AUROC and FPR95 in % are given. The hyperparameters β and α are set as [0.4, 0.6] and 0.1.

Backbone	Ratio	Closed-Set Metric	Open-Set Metric		
		Accuracy (sample)	FPR (95% TPR) \downarrow	Detection Error \downarrow	AUROC \uparrow
PointNet++ [8]	0.01	97.9	33.4	14.7	85.9
	0.05	97.8	35.4	15.5	86.2
	0.1	97.7	35.4	15.6	86.4
	0.2	97.8	34.2	15.0	86.1
	0.3	97.4	42.0	16.2	84.8
	0.5	97.2	43.0	17.1	84.3

Table 11: **Performance drop:** Open-Set Point Cloud Classification of PointNet++ on ModelNet40-Split with different ratios of using samples as unknown ones.